Metabolic Control of Viral Infection through PPAR-α Regulation of STING Signaling

Lili Tao[1], Alexandria Lowe[1], Guoxun Wang[1], Igor Dozmorov[1], Tyron Chang[1], Nan Yan[1,2], Tiffany A. Reese[1,2*]

[1]Department of Immunology, University of Texas Southwestern Medical Center, Dallas, TX, 75390, USA
[2]Department of Microbiology, University of Texas Southwestern Medical Center, Dallas, TX, 75390, USA

*corresponding author

Abstract

Peroxisomal proliferator activated receptors (PPARs) are sensors of dietary lipids and pharmacological targets in the treatment of metabolic disorders. However, PPAR ligands are immunosuppressive and can increase susceptibility to infection. Moreover, the specific mechanisms that underlie the immunoregulatory properties of PPARs remain unclear. We investigated the consequences of PPAR activation during herpesvirus infection. We found that activation of PPAR-α with specific agonists increased herpesvirus replication and reactive oxygen species (ROS) production. ROS inhibited activation of stimulator of interferon (STING), an ER adapter that induces type I interferon downstream of cytoplasmic DNA recognition. Although high ROS induces inflammasome activation and cytokine production, we found that ROS inhibited interferon production. Treatment of mice with a clinically relevant agonist of PPAR-α increased herpesvirus replication and pathogenesis, comparable to levels observed previously in type I interferon receptor knockout mice. These findings show that activated PPAR-α regulates immunity to cytoplasmic DNA, inhibits interferon production, and increases susceptibility to viral infection. Moreover, these results demonstrate that ROS inhibit STING activation and induction of interferon.

33

34 **Introduction**

35

36 Peroxisome proliferator activated receptors (PPARs) are ligand activated nuclear
37 receptors that regulate fatty acid oxidation and cholesterol metabolism. The PPAR family
38 consists of three isoforms: PPAR-α, PPAR-β/δ, and PPAR-γ. All three receptors regulate lipid
39 homeostasis, although they differ in terms of their tissue distribution, ligand specificities, and
40 gene targets [1]. There are many natural and synthetic ligands of PPARs that are used to treat
41 dyslipidemia and glucose disorders. Natural ligands include dietary lipids, such as omega-3
42 polyunsaturated fatty acids found in fish oil, and immune mediators, such as eicosanoids.
43 Synthetic ligands, including fibrates that target PPAR-α and thiazolidinediones that target
44 PPAR-γ, are used to treat metabolic disorders [1,2].

45 In addition to their role in metabolism, PPARs regulate inflammation. PPAR agonists
46 reduce inflammation in atherosclerosis, diabetes, neurodegenerative diseases, and autoimmune
47 diseases [3]. Their mechanisms of action are diverse and include repression of NFκB and AP-1
48 DNA binding, regulation of nitric oxide, inhibition of dendritic cell maturation, reduction of
49 cytokine expression by effector T cells, and inhibition of leukocyte recruitment to sites of
50 inflammation [4,5]. Despite their immunosuppressive function, the effects of PPAR agonists on
51 infectious disease outcomes has not been extensively studied. There are some reports that
52 synthetic agonists or dietary lipids improve or impair resistance to pathogen challenge, but we
53 do not know the molecular mechanisms of PPAR-mediate immunoregulation during infection [6–
54 10].

55 Intermediates of cellular metabolism are important signaling molecules that alter immune
56 defense pathways [11]. PPARs, as their name implies, increase peroxisomal metabolism.
57 Peroxisomes synthesize phospholipids and bile acids and oxidize very long, branched chain,

58 and polyunsaturated fatty acids. They also produce significant amounts of hydrogen peroxide
59 and other reactive oxygen species (ROS). ROS have been widely implicated in inflammatory
60 processes, particularly for NFκB signaling and inflammasome activation [12]. In general,
61 antioxidant treatment reduces inflammatory cytokines and interferon-β (IFNβ) after stimulation
62 with toll-like receptor agonists or viral RNA [13–16]. However, it is unclear whether peroxisomal
63 metabolism and ROS function in antiviral immunity to DNA viruses and cytoplasmic DNA.
64 Herpesviruses manipulate metabolism during infection to promote viral replication and
65 chronic infection [17,18]. In addition to altering glucose metabolism, herpesviruses induce
66 peroxisome proliferation [19,20]. Moreover, they encode viral proteins that target peroxisomes,
67 suggesting that modulation of peroxisomal function is important for these viruses [21–23].
68 Here we investigated the consequences of activation of PPARs and peroxisomal
69 metabolism on herpesvirus infection and induction of antiviral immune responses. We
70 compared agonists for the three different PPARs and found that activation of PPAR-α increased
71 herpesvirus replication. PPAR-α stimulation inhibited type I interferon production following
72 DNA-virus infection or direct stimulation of the cyclic GMP-AMP synthase (cGAS)/stimulator of
73 interferon (STING) pathway. Importantly, treatment of mice with PPAR-α agonist led to
74 increased herpesvirus replication and heightened lethality in agonist-treated mice. Our data
75 suggest that activation of PPAR-α suppresses cytoplasmic DNA sensing by generating high
76 ROS that inhibit STING activation, leading to reduced type I interferon and impaired immunity to
77 viral infections.
78
79 **Results**
80 *Activation of PPAR-α promotes MHV68 replication.*
81

82 To examine the effects of PPAR activation on DNA virus infection, we used murine
83 gammaherpesvirus-68 (MHV68) as our model. MHV68 readily infects mice and undergoes
84 phases of infections similar to human herpesvirus, such as Kaposi's sarcoma associated
85 herpesvirus (KSHV) and Epstein Barr virus (EBV) [24–26]. We treated bone marrow derived
86 macrophages with PPAR-α agonists, fenofibrate or WY14643, PPAR-β/δ agonist GW501516, or
87 PPAR-γ agonist rosiglitazone. Following pretreatment, cells were infected with MHV68. We
88 examined expression of lytic viral proteins on infected cells by flow cytometry to assay for viral
89 replication [25]. We found that PPAR-α agonists fenofibrate and WY14643 both increased
90 expression of lytic viral proteins on infected macrophages compared with untreated cells or cells
91 treated with GW501516 or rosiglitazone (Figure 1a). MHV68 replication at either low or high
92 multiplicity of infection (MOI) was also increased in macrophages treated with fenofibrate or
93 WY14643 compared with untreated cells (Figure 1b, c, Supplemental Figure 1). Treatment with
94 agonist had no effect on virus replication in macrophages isolated from *Ppara*$^{-/-}$ mice,
95 suggesting that PPAR-α is critical for agonist effects (Figure 1d). We tested whether stimulation
96 of PPAR-α affected replication of another herpesvirus that also infects macrophages and found
97 that replication of murine cytomegalovirus (MCMV) was also increased by PPAR-α agonist
98 (Supplemental Figure 2). Thus, PPAR-α stimulation increases herpesvirus replication in a
99 PPAR-α-dependent manner.
100
101 *PPAR-α stimulation suppresses type I IFN production in a STING-dependent manner*
102
103 To broadly assess the impact of PPAR-α agonist on cells infected with virus, we
104 performed RNA sequencing analysis on macrophages infected with virus and treated with
105 WY14643. Six hours after infection, uninfected/vehicle treated, MHV68+/vehicle treated,
106 uninfected/WY14643 treated cells, and MHV68+/WY14643 treated macrophages were prepared

107 for RNA-seq. Pathway analysis of differentially expressed genes revealed that virus infection in
108 both vehicle-treated and WY14643-treated cells increased expression of interferon responsive
109 genes, genes involved in inflammation, and NFκB pathway genes (Figure 2a, Supplemental
110 Table 1). However, PPAR-α stimulation reduced the magnitude of upregulation in infected cells.
111 Thus, PPAR-α stimulation attenuates the early antiviral response in infected cells.

112 To confirm the sequencing results, we quantified expression of a subset of interferon
113 stimulated genes. We measured *Isg20*, *Isg15*, and *Cxcl10* and confirmed that expression of
114 these genes is reduced in both uninfected and infected macrophages treated with WY14643
115 (Figure 2b). We also measured expression of *Ifnb* and found that expression is reduced after
116 agonist treatment (Figure 2b). These data suggest that PPAR-α stimulation suppresses the
117 interferon response at baseline and after viral infection.

118 Because of the suppression of the early antiviral response, we tested whether the effects
119 of PPAR-α stimulation depended on the type I interferon response. To test this, we examined
120 viral growth in wildtype and *Ifnar*$^{-/-}$ macrophages with and without agonist treatment. As
121 expected, virus grew substantially more in *Ifnar*$^{-/-}$ cells compared with wildtype cells. PPAR-α
122 stimulation did not further increase virus replication in the knockout cells (Supplemental Figure
123 3). Thus, PPAR-α stimulation effects depend on type I interferon.

124 MHV68 is a DNA virus that induces interferon downstream of the cGAS/STING pathway;
125 therefore, we hypothesized that PPAR-α stimulation could antagonize the early induction of
126 interferon after recognition of cytoplasmic DNA. Cytoplasmic DNA is sensed by cGAS, leading
127 to activation of endoplasmic reticulum adapter molecule STING. STING phosphorylates TBK1
128 and IRF3, leading to transcription of IFNβ. IFNβ then signals through the type I IFN receptor to
129 induce interferon stimulated gene expression and more IFNβ expression. To test if PPAR-α
130 stimulation could suppress IFNβ induction after direct activation of STING, macrophages were
131 treated with vehicle or agonist and stimulated with DMXAA, a murine agonist of STING. We

132 found that PPAR-α stimulation suppressed IFNβ expression after DMXAA transfection (Figure
133 2c). As expected, the PPAR-γ and PPAR-δ agonists rosiglitazone and GW501516 did not
134 suppress IFNβ expression after DMXAA treatment (Supplemental Figure 4). Moreover, PPAR-α
135 stimulation suppressed production of IFNβ protein (Figure 2d). These data suggest that PPAR-
136 α stimulation antagonizes the induction of interferon production downstream of the STING DNA
137 sensing pathway.

138 To test if suppression of IFNβ depended on STING, we treated *Sting*$^{-/-}$ macrophages
139 with PPAR-α agonist and infected with MHV68. We found that PPAR-α stimulation no longer
140 increased virus replication in cells deficient in STING (Figure 2e). We examined activation of
141 TBK1 and IRF3 and found that PPAR-α stimulation suppressed DMXAA-induced
142 phosphorylation of both proteins (Figure 2f). These data indicate that the effects of PPAR-α
143 agonist depend on STING expression and suggest that PPAR-α stimulation antagonizes the
144 initial induction of IFNβ after recognition of cytoplasmic DNA.

145

146 *PPAR-α stimulation induces oxidative stress*

147

148 We wondered if PPAR-α agonist effects could promote virus replication even if cells
149 were treated with agonist after infection, or if the effects of agonist required pretreatment. To
150 test this, we compared three different treatment protocols. We pretreated, as above, with
151 PPAR-α agonist overnight and replaced agonist in the media following infection with MHV68.
152 We compared this with pretreatment only (pre) or post treatment only (post). We found that
153 pretreatment with PPAR-α agonist was required to increase MHV68 replication (Figure 3a). We
154 found no increase in virus replication when cells were treated post-infection with agonist. We
155 also found that pretreatment alone was sufficient to increase virus replication. These data

156 suggest that PPAR-α stimulation is altering the cellular environment prior to infection in such a
157 way that enhances virus replication.

158 In order to determine how PPAR-α stimulation was altering the cellular environment to
159 promote virus replication and impair interferon induction, we examined vehicle and WY14643-
160 only treatments from our sequencing data. PPAR-α agonist treated cells displayed increased
161 antioxidant response pathways, indicating a possible increase in oxidative stress in PPAR-α
162 agonist treated cells (Figure 3b, Supplemental Table 2). To confirm these results, we analyzed
163 expression of antioxidant genes in untreated or PPAR-α agonist treated macrophages and
164 confirmed increased expression of *Mgst1*, *Gsr*, *Slc7a11*, *Gstm1*, *Gclm*, and *Cd36* in agonist
165 treated cells (Figure 3c). PPAR-α agonist treatment of macrophages also promoted increase
166 total ROS (Figure 3d). These results are comparable to previous data indicating that PPAR-α
167 agonist treatment increases β-oxidation of fatty acids in peroxisomes and enhances production
168 of ROS [27,28].

169 Given that PPAR-α stimulation increased antioxidant gene expression and ROS
170 production and that these effects correlated with increased viral replication, we next tested
171 whether increased ROS suppressed IFNβ production. Macrophages were treated with
172 hydrogen peroxide (H_2O_2) and stimulated with DMXAA. H_2O_2 treatment suppressed DMXAA-
173 induced IFNβ production (Figure 3e). In addition, N-Acetyl-L-cysteine (NAC), an antioxidant,
174 partially neutralized the effects of H_2O_2 (Figure 3e). H_2O_2 treatment suppressed
175 phosphorylation of TBK1 and IRF3 (Figure 3f). This indicates that increased oxidative stress
176 suppresses the cGAS/STING pathway after activation with cytoplasmic DNA.

177 To determine if cells that have constitutive high levels of ROS have impaired interferon
178 responses, we examined that antiviral response in nuclear factor E2-related factor 2 (NRF2)
179 deficient cells. NRF2 is a transcription factor that regulates antioxidant responses by binding to
180 antioxidant response elements (ARE) found in promoters of detoxication enzymes. NRF2

181 activity is regulated by KEAP1, and KEAP1 under non-stressed conditions promotes NRF2
182 ubiquitylation. When cells are under oxidative stress, NRF2 is released from KEAP1 and drives
183 antioxidant gene expression [29]. *Nrf2*$^{-/-}$ cells do not induce antioxidant genes and have high
184 levels of ROS [30–32]. We confirmed that *Nrf2*$^{-/-}$ macrophages had increased ROS (Figure 3g).
185 When we stimulated *Nrf2*$^{-/-}$ macrophages with DMXAA they induced less *Ifnb* expression
186 compared to wildtype cells (Figure 3H). Additionally, PPAR-α agonists did not further suppress
187 *Ifnb* transcript production from knockout cells (Figure 3h). Together, these data suggest that
188 ROS can suppress IFNβ downstream of direct STING activation.
189 To determine if the lower levels of IFNβ expressed in *Nrf2*$^{-/-}$ macrophages led to
190 increased viral replication, we infected *Nrf2*$^{-/-}$ and wildtype macrophages with MHV68. We
191 observed increase viral protein expression after infection in *Nrf2*$^{-/-}$ macrophages, indicating that
192 virus replicated better in cells with higher levels of ROS and decreased IFNβ (Figure 3i).
193
194 *PPAR-α stimulation increases virus replication and lethality in mice.*
195
196 Because we found that PPAR-α stimulation *in vitro* suppressed interferon production, we
197 hypothesized that agonist treatment of mice infected with MHV68 would alter herpesvirus
198 replication. Previously published work established that mice deficient in the IFNα/β receptor
199 (IFNAR) have increased viral replication and enhanced susceptibility to MHV68 [33]. To
200 determine if PPAR-α stimulation increased MHV68 replication *in vivo,* we injected wildtype and
201 *Ppara*$^{-/-}$ mice with WY14643 or vehicle control for 7 days, starting 3 days prior to infection and
202 continuing for 4 days after infection (Figure 4a). Mice were infected with a dose of MHV68 that
203 does not cause lethality in wildtype mice treated with the drug vehicle. However, wildtype mice
204 injected with PPAR-α agonist succumbed to infection (Figure 4b), at a frequency similar to type I
205 interferon receptor deficient mice [33]. Moreover, *Ppara*$^{-/-}$ mice treated with agonist or vehicle all

206 survived infection with MHV68, indicating that the lethality observed in wildtype mice treated
207 with agonist is PPAR-α dependent (Figure 4c). Using a luciferase-tagged MHV68 (MHV68-
208 M3FL) we imaged mice infected with virus over multiple days during acute infection [25,34]. We
209 found that mice treated with WY14643 had increased virus replication compared to vehicle
210 treated mice, and that this increase in virus replication was PPAR-α dependent (Figure 4d, e).
211 These data suggest that PPAR-α stimulation significantly increased MHV68 acute replication.
212 To determine if the interferon response was altered by PPAR-α stimulation, we analyzed
213 interferon stimulated gene expression in the peritoneal cells for vehicle-treated and agonist-
214 treated mice. We found that expression of *Isg20* and *Cxcl10* was decreased in agonist treated
215 mice (Figure 4f), indicated that treatment with PPAR-α agonist during acute infection
216 suppressed the interferon response.
217
218 **Discussion**
219
220 We determined that activation of PPAR-α with clinically relevant agonists increases
221 herpesvirus replication. In macrophages, PPAR-α stimulation increased virus replication and
222 suppressed the induction of an interferon response in a STING-dependent manner. PPAR-α
223 stimulation induced oxidative stress in cells and high levels of oxidative stress impaired STING
224 activation. This is the first evidence that PPAR-α activation and peroxisomal metabolism
225 regulate the cytoplasmic DNA-sensing pathway and IFNβ production downstream of STING.
226 PPAR-α stimulation significantly increased herpesvirus replication in mice, leading to increased
227 lethality of agonist-treated mice.
228 Metabolism is recognized as an important regulator of immunity. Metabolic
229 reprogramming of macrophages, in particular, is essential for modifying their inflammatory
230 phenotype and function. Glycolysis drives inflammatory macrophage responses, whereas high

231 fatty acid oxidation was long thought to support anti-inflammatory macrophage responses [35]. It
232 is now clear that fatty acid oxidation is not just anti-inflammatory, because oxidation of palmitate
233 promotes the production of mitochondrial ROS, which induces inflammasome activation [36,37].
234 Moreover, mitochondrial ROS promotes the production of the proinflammatory cytokines IL-1β,
235 IL-6, and TNFα following LPS stimulation of macrophages [38]. Our data adds another level of
236 complexity to the role of ROS in inflammation. Our data indicates that ROS, perhaps derived
237 from peroxisomal β-oxidation of very long chain fatty acids or other sources, impairs STING
238 activation and interferon production. Further work is needed to determine the source of ROS.
239 However, our data thus far suggests that the induction of peroxisomal metabolism and fatty acid
240 oxidation impairs innate immune signaling.
241 These data reveal that peroxisomal metabolism and increased ROS production
242 regulates the cytoplasmic DNA sensing pathway. The adapter molecule MAVS that signals
243 downstream of RNA recognition is localized to mitochondria and peroxisomes. Interestingly, the
244 peroxisomal localization of MAVS dictates unique signaling pathways and gene responses
245 distinct from mitochondrial MAVS [39,40]. Together these data along with our data indicate that
246 peroxisomes are critical organelles for the induction of innate immune signals, either through
247 localization of signaling molecules or production of metabolites that regulate immune signaling.
248 Herpesviruses use multiple mechanisms to maintain chronic infections in the host and
249 peroxisomal metabolism is a putative mechanism. To avoid clearance, herpesviruses evade
250 immune recognition by downregulating antigen presentation, expressing viral proteins that
251 regulate the interferon pathway, inhibiting cell cycle arrest and apoptosis, and encoding various
252 molecular mimics. This is indicative of a long evolutionary relationship with the host. It also
253 suggests that herpesviruses modify numerous pathways within the host cell to tune the balance
254 between latency and reactivation. Peroxisomal proliferation is a feature of herpesvirus infection,
255 but the function of peroxisomal biogenesis during latency has been elusive. A recent report

256 found that HCMV and HSV-1 induced peroxisome biogenesis and plasmalogen production,
257 leading to enhanced virus envelopment and lytic replication [20]. However, these data do not
258 address the potential role of peroxisome biogenesis in chronic infection with a herpesvirus.
259 KSHV latent cell survival requires peroxisomal lipid metabolism, suggesting that KSHV
260 regulates peroxisomal lipid metabolism to support latent infection [19]. One hypothesis is that
261 peroxisomes and the redox balance of the cell control latency by adjusting the production of
262 type I interferon.

263 A key remaining question is how ROS regulates STING activation. Recent structural
264 data provide numerous insights into the mechanism of cGAMP activation of STING [41,42]. STING
265 dimers in the ER form polymers upon binding to cGAMP and disulfide bonds in the cytosolic
266 domain stabilize STING polymers. These inter-dimer crosslinks are important for STING
267 activation. One possibility is that increased oxidative stress leads to oxidation of cysteine
268 residues in the cytosolic domain, which interferes with the polymerization and activation of
269 STING [43].

270 Overall, our work suggests that activation of PPAR-α suppresses interferon and antiviral
271 immunity. Moreover, these data indicate that metabolism and particularly ROS have both
272 proinflammatory and anti-inflammatory functions. These results have implications for therapies
273 that target PPAR-α or oxidative stress pathways for the treatment of infection, metabolic
274 disorders, cancer and autoimmune disease.

275

276 **Acknowledgments**

277 We thank members of the Reese and Yan labs for technical assistance, David
278 Mangelsdorf and Steven Kleiwer for reagents and expertise, Dr. Wenhan Zhu for help with data
279 analysis, and Drs. Julie Pfeiffer and Lora Hooper for editorial assistance. We also thank the
280 UTSW Flow Cytometry core and the Genomic and Microarray core for technical assistance.

The Reese lab is supported by the American Heart Association (17SDG33670071), the NIH (1R01AI130020-01A1), and the Pew Scholars Program.

Author Contributions

L.T. performed and analyzed experiments, with technical assistance from A.L, G.W and T.C. I.D. performed RNAseq analysis. N.Y. provided reagents and expertise. T.A.R. directed the project and wrote the manuscript.

Declaration of Interests

The authors declare no competing interests.

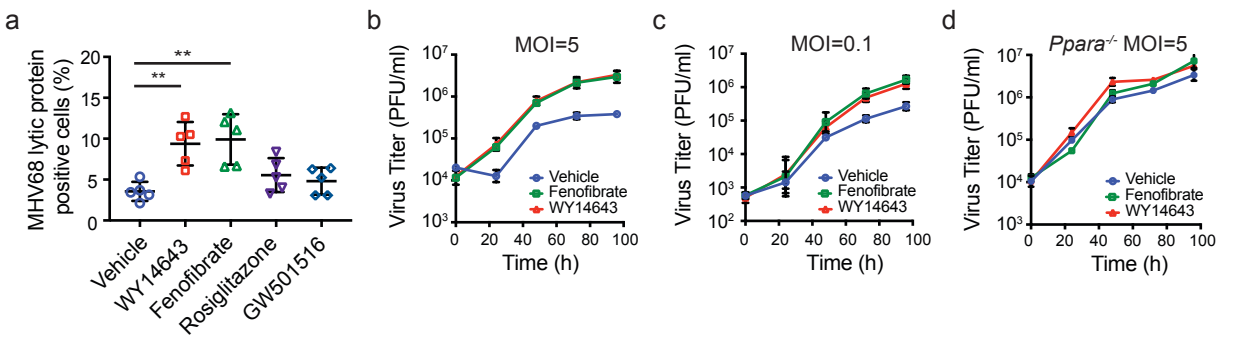
a
MHV68 lytic protein positive cells (%)
20
15
10
5
0
**
**
Vehicle
WY14643
Fenofibrate
Rosiglitazone
GW501516
b
MOI=5
Virus Titer (PFU/ml)
10^7
10^6
10^5
10^4
10^3
0 20 40 60 80 100
Time (h)
Vehicle
Fenofibrate
WY14643
c
MOI=0.1
Virus Titer (PFU/ml)
10^7
10^6
10^5
10^4
10^3
10^2
0 20 40 60 80 100
Time (h)
Vehicle
Fenofibrate
WY14643
d
Ppara$^{-/-}$ MOI=5
Virus Titer (PFU/ml)
10^7
10^6
10^5
10^4
10^3
0 20 40 60 80 100
Time (h)
Vehicle
Fenofibrate
WY14643

292 **Figure 1. PPAR-α stimulation increases MHV68 replication.**

293 a, Macrophages from C57BL6/J mice were pretreated for 16 hours with WY14643, fenofibrate,
294 rosiglitazone, or GW501516. Cells were infected with MHV68 at MOI=5. Quantification of cells
295 expressing MHV68 lytic proteins using a polyclonal antibody 24 hours after infection was
296 measured by flow cytometry. Data represents mean ± SD from 5 independent experimental.

297 b-c, Growth curve of MHV68 in macrophages isolated from C57BL/6J mice after pretreatment
298 with vehicle, WY14643 or fenofibrate. Cells were infected with MHV68 at MOI=5 (b) or MOI=0.1
299 (c). Virus quantitated by plaque assay on 3T12 cells. Data represents mean ± SD from 3
300 independent experiments.

301 d, Growth curve of MHV68 in macrophages isolated from *Ppara*$^{-/-}$ mice after pretreatment with
302 vehicle, WY14643 or fenofibrate. Cells were infected with MHV68 at MOI=5. Data represents
303 mean ± SD from 3 independent experiments.

304

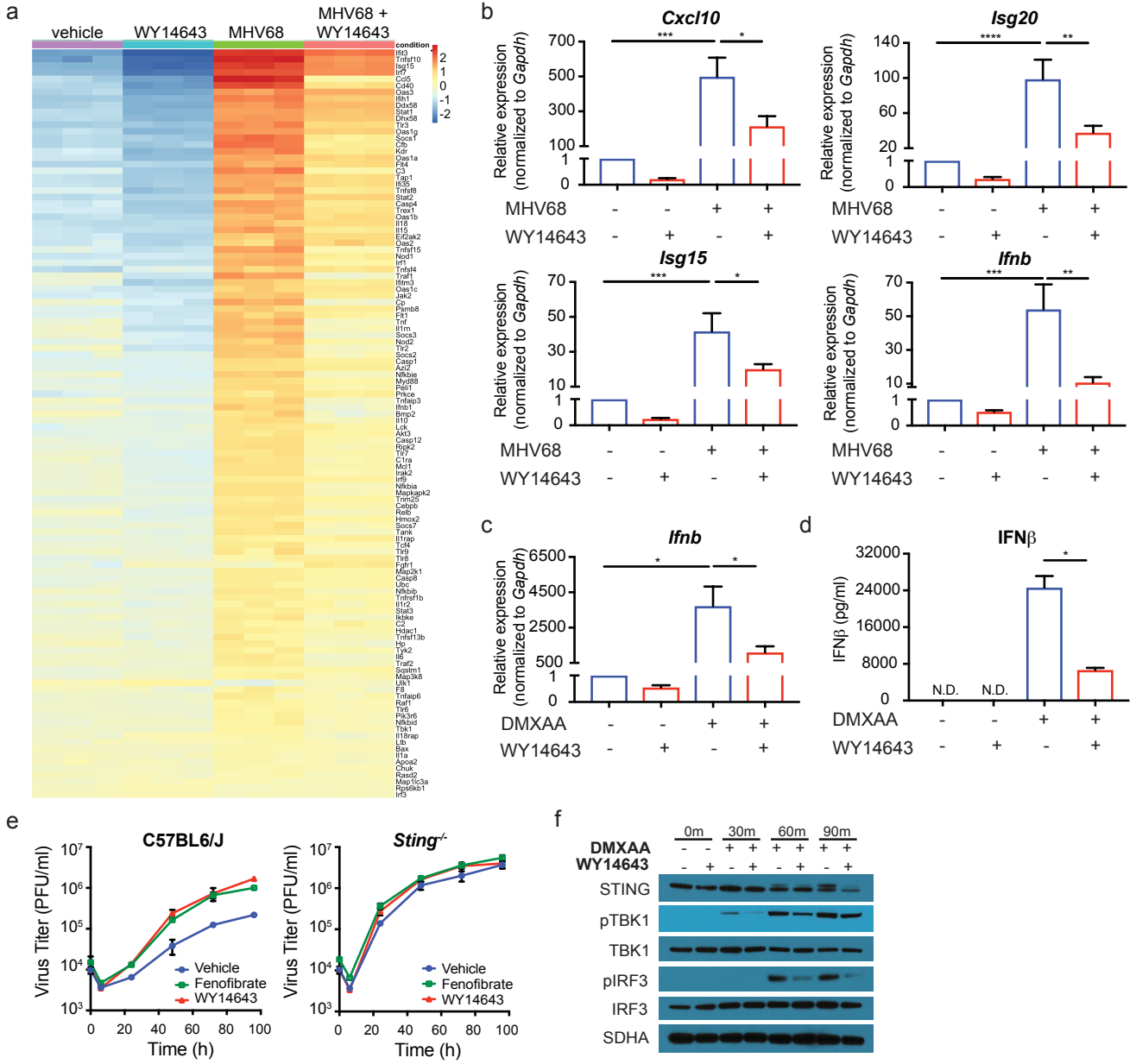
a
vehicle
WY14643
MHV68
MHV68 + WY14643
condition
2
1
0
-1
-2
b
Cxcl10
Isg20
Isg15
Ifnb
Relative expression (normalized to Gapdh)
MHV68
WY14643
c
Ifnb
DMXAA
d
IFNβ
IFNβ (pg/ml)
N.D.
e
C57BL6/J
Sting-/-
Virus Titer (PFU/ml)
Time (h)
Vehicle
Fenofibrate
WY14643
f
0m
30m
60m
90m
DMXAA
WY14643
STING
pTBK1
TBK1
pIRF3
IRF3
SDHA

305 **Figure 2. PPAR-α stimulation suppresses type I IFN in a STING-dependent manner.**
306
307 a, Macrophages were pretreated with vehicle or WY14643 for 16 hours prior to infection with
308 MHV68, MOI=5. 6 hours after infection, RNA was isolated and prepared for RNA sequencing.
309 b, Macrophages were pretreated with vehicle or WY14643 for 16 hours prior to infection with
310 MHV68. qRT-PCR of *Cxcl10*, *Isg20*, *Isg15* and *Ifnb* before and 6 hours after MHV68 infection.
311 Relative expression normalized to *Gapdh*. n=5 for *cxcl10*, n=7 for *Isg20*, n=6 for *Isg15*, n=8 for
312 *Ifnb.*
313 c, Macrophages were pretreated with vehicle or WY14643 for 16 hours prior to transfection with
314 DMXAA. qRT-PCR of *Ifnb* before and 2 hours after transfection with DMXAA. Relative
315 expression normalized to *Gapdh*. n=9.
316 d, Macrophages were pretreated with vehicle or WY14643 for 16 hours prior to transfection with
317 DMXAA. Concentration of IFNβ in culture medium before and 24 hours after transfection was
318 determined by ELISA assay. n=3.
319 e, Macrophages from C57BL6/J or *Sting*$^{-/-}$ mice were pretreated with vehicle or WY14643 for 16
320 hours prior to infection with MHV68, MOI=5. Virus growth was quantitated by plaque assay.
321 n=3.
322 f, Macrophages were pretreated with vehicle or WY14643 for 16 hours. Representative western
323 blot of proteins involved in STING signaling before transfection and 30 mins, 60 mins, 90 mins
324 after transfection with DMXAA.
325 Data all shown as mean ± SD; $^{*}p<0.05$, $^{**}p<0.01$, $^{***}P<0.001$, statistical analysis was conducted
326 using one-way ANOVA test.
327

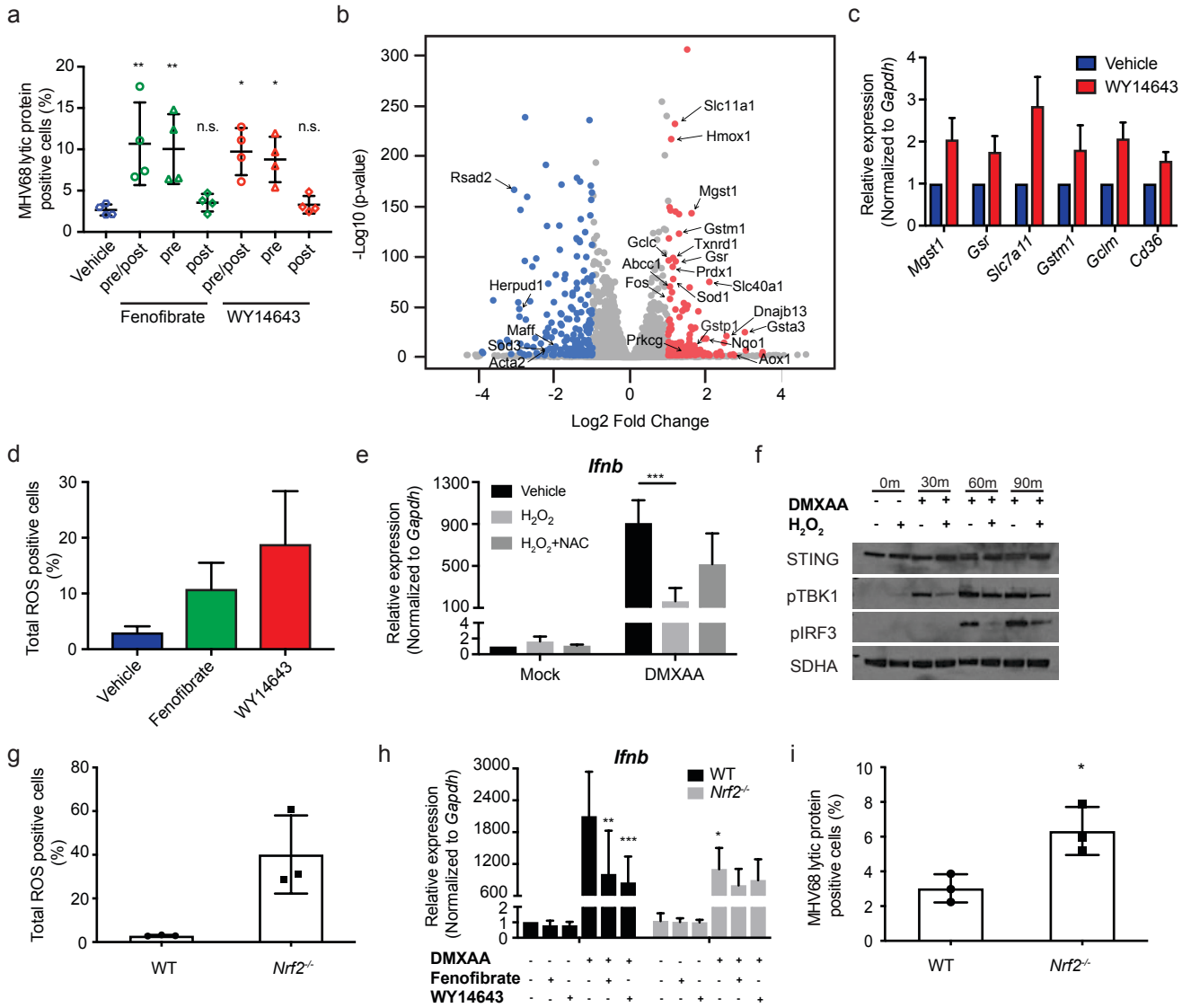
a
MHV68 lytic protein positive cells (%)
Vehicle
pre/post
pre
post
pre/post
pre
post
Fenofibrate
WY14643
n.s.
b
-Log10 (p-value)
Log2 Fold Change
Slc11a1
Hmox1
Rsad2
Mgst1
Gstm1
Gclc
Txnrd1
Gsr
Abcc1
Prdx1
Herpud1
Fos
Slc40a1
Sod1
Dnajb13
Maff
Gstp1
Gsta3
Sod3
Prkcg
Nqo1
Acta2
Aox1
c
Relative expression (Normalized to Gapdh)
Vehicle
WY14643
Mgst1
Gsr
Slc7a11
Gstm1
Gclm
Cd36
d
Total ROS positive cells (%)
Vehicle
Fenofibrate
WY14643
e
Ifnb
Relative expression (Normalized to Gapdh)
Vehicle
H2O2
H2O2+NAC
Mock
DMXAA
f
0m
30m
60m
90m
DMXAA
H2O2
STING
pTBK1
pIRF3
SDHA
g
Total ROS positive cells (%)
WT
Nrf2-/-
h
Ifnb
Relative expression (Normalized to Gapdh)
WT
Nrf2-/-
DMXAA
Fenofibrate
WY14643
i
MHV68 lytic protein positive cells (%)
WT
Nrf2-/-

328

329 **Figure 3. Oxidative stress inhibits STING activation and interferon production.**

330 a, Macrophages were treated with vehicle, WY14643 or fenofibrate agonist pre and post-
331 infection (pre/post), pre-infection only (pre) or post-infection only (post). Quantification of cells
332 expressing MHV68 lytic proteins by FACs assay 24 hours after infection. n=4.

333 b, Comparison of vehicle-treated or WY14643-treated macrophages from RNA sequencing
334 analysis in Figure 2A.

335 c, Macrophages were treated with either vehicle control or WY14643 overnight. Genes
336 associated with oxidative stress response were quantitated by qRT-PCR. Relative expression
337 normalized to *Gapdh*. n=5 from independent experiments.

338 d, Macrophages were treated with vehicle, fenofibrate or WY14643 for 6 hours. Quantification
339 of total ROS in BMDMs by flow cytometry. n=7 with vehicle and fenofibrate treatment, n=6 with
340 WY14643 treatment.

341 e, Macrophages were pretreated with vehicle control or H_2O_2 for 20 mins. Half of the H_2O_2
342 samples were treated with NAC for 30 minutes and half were mock treated. Treatments were
343 replaced with fresh media and cells were transfected with DMXAA. After 2 hours *Ifnb* was
344 quantitated from lysates by qRT-PCR. n=4 from independent experiments.

345 f, Macrophages were treated with either vehicle or H_2O_2 for 20 mins, and then transfected with
346 DMXAA. Expression of STING, phosphorylated TBK1 (pTBK1), phosphorylated IRF3 (pIRF3),
347 and SDHA was quantitated 0, 30, 60 or 90 minutes after transfection. Representative of 3
348 separate experiments.

349 g, Macrophages were isolated from C57BL6/J or *Nrf2*$^{-/-}$ mice. Total ROS was quantitated by flow
350 cytometry. n=3 from independent experiments.

351 h, Macrophages isolated from WT or *Nrf2*$^{-/-}$ mice were pretreated for 16 hours with fenofibrate,
352 WY14643, or vehicle. Cells were transfected with DMXAA and expression of *Ifnb* transcript was
353 quantitated 2 hours later. Relative expression of *Ifnb* was normalized to *Gapdh*. n=5

354 Data all shown as mean ± SD; $^{*}p<0.05$, $^{**}p<0.01$, $^{***}P<0.001$, statistical analysis was conducted

355 using one-way ANOVA or two-way ANOVA test.

356 i, Macrophages isolated from WT or *Nrf2*$^{-/-}$ mice were infected with MHV68 at a MOI=5 for 24

357 hours. Cells expressing MHV68 lytic proteins were quantified by FACs assay. N=3 from

358 independent experiments.

359 Data all shown as mean ± SD; $^{*}p<0.05$, $^{**}p<0.01$, statistical analysis was conducted using one-

360 way ANOVA or unpaired t-test.

361

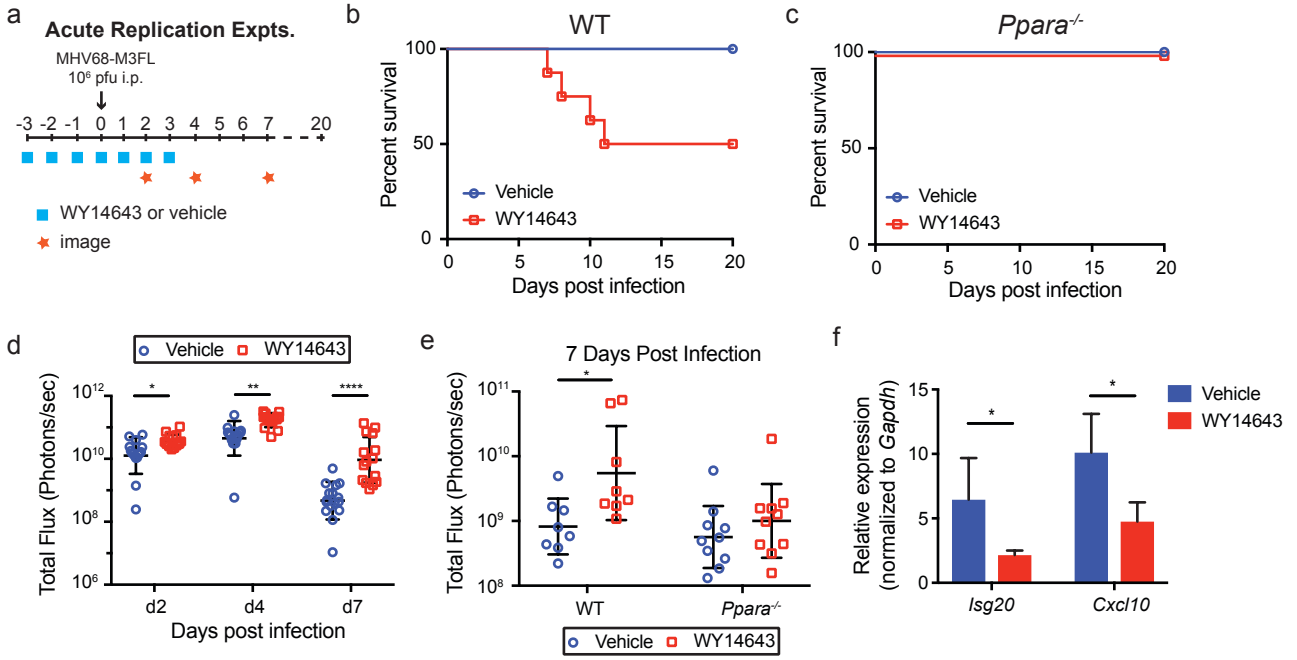
a
Acute Replication Expts.
MHV68-M3FL
10⁶ pfu i.p.
-3 -2 -1 0 1 2 3 4 5 6 7 20
WY14643 or vehicle
image
b
WT
Percent survival
Vehicle
WY14643
Days post infection
c
Ppara-/-
Percent survival
Vehicle
WY14643
Days post infection
d
Vehicle
WY14643
Total Flux (Photons/sec)
d2
d4
d7
Days post infection
e
7 Days Post Infection
Total Flux (Photons/sec)
WT
Ppara-/-
Vehicle
WY14643
f
Relative expression
(normalized to Gapdh)
Isg20
Cxcl10
Vehicle
WY14643

362 **Figure 4. PPAR-α stimulation in mice increases virus replication and lethality.**

363 a, Schematic for acute replication of MHV68 in mice. Mice were treated with either vehicle
364 control (15% HS15) or WY14643 (100 mg/kg) for 7 days, starting 3 days before infection. Mice
365 were infected intraperitoneally with MHV68-M3FL at dose of 10^6 PFU. Acute replication of virus
366 was measured at d2, d4 and d7 after infection using an IVIS bioluminescent imager. Survival of
367 mice was monitored until 20 days after infection.

368 b-c, Survival of mice infected with MHV68. C57BL6/J (b) or *Ppara*$^{-/-}$ (c) mice were treated with
369 either vehicle control or WY14643, and infected with MHV68. n=8 in each group of C57BL6/J
370 mice, n=10 in each group of *Ppara*$^{-/-}$ mice. Data shown as the pool of 2 independent
371 experiments.

372 d, Acute replication of MHV68 in mice measured by luminescent intensity. n=16 in vehicle
373 treatment group, n=15 in WY14643 treatment group, data shown as the pool of 3 independent
374 experiments.

375 e, Acute replication of MHV68 in WT or *Ppara*$^{-/-}$ mice measured by luminescent intensity. n=8 in
376 each group of WT mice, n=10 in each group of *Ppara*$^{-/-}$ mice. Data shown as the pool of 2
377 independent experiments.

378 f, Peritoneal exudate cells were collected from vehicle or WY14643-treated mice 2 days after
379 infection with MHV68. Relative expression of *Isg20* and *Cxcl10* was quantitated and normalized
380 to *Gapdh*. n=4 from 2 independent experiments.

381 Data all shown as mean ± SD; $^{*}p<0.05$, $^{**}p<0.01$, $^{***}P<0.001$, statistical analysis was conducted
382 using one-way ANOVA or two-way repeated measures ANOVA test.

383

References

1. Grygiel-Górniak, B. Peroxisome proliferator-activated receptors and their ligands: nutritional and clinical implications--a review. *Nutrition journal* **13,** 17 (2014).

2. Staels, B. *et al.* Mechanism of action of fibrates on lipid and lipoprotein metabolism. *Circulation* **98,** 2088–2093 (1998).

3. Staels, B. & Fruchart, J.-C. C. Therapeutic roles of peroxisome proliferator-activated receptor agonists. *Diabetes* **54,** 2460–70 (2005).

4. Bensinger, S. J. & Tontonoz, P. Integration of metabolism and inflammation by lipid-activated nuclear receptors. *Nature* **454,** 470–477 (2008).

5. Straus, D. S. & Glass, C. K. Anti-inflammatory actions of PPAR ligands: new insights on cellular and molecular mechanisms. *Trends in immunology* **28,** 551–558 (2007).

6. Husson, M.-O. O. *et al.* Modulation of host defence against bacterial and viral infections by omega-3 polyunsaturated fatty acids. *The Journal of infection* **73,** 523–535 (2016).

7. Jones, G. J. & Roper, R. L. The effects of diets enriched in omega-3 polyunsaturated fatty acids on systemic vaccinia virus infection. *Scientific reports* **7,** 15999 (2017).

8. Manoharan, I. *et al.* Homeostatic PPARα Signaling Limits Inflammatory Responses to Commensal Microbiota in the Intestine. *Journal of immunology (Baltimore, Md. : 1950)* **196,** 4739–4749 (2016).

9. Anderson, M. & Fritsche, K. L. (n-3) Fatty acids and infectious disease resistance. *The Journal of nutrition* **132,** 3566–76 (2002).

10. Irons, R., Anderson, M. J., Zhang, M. & Fritsche, K. L. Dietary fish oil impairs primary host resistance against Listeria monocytogenes more than the immunological memory response. *The Journal of nutrition* **133,** 1163–9 (2003).

11. O'Neill, L. A., Kishton, R. J. & Rathmell, J. A guide to immunometabolism for immunologists. *Nature Reviews Immunology* **16,** 553–565 (2016).

12. Forrester, S. J., Kikuchi, D. S., Hernandes, M. S., Xu, Q. & Griendling, K. K. Reactive Oxygen Species in Metabolic and Inflammatory Signaling. *Circulation research* **122,** 877–902 (2018).

13. Soucy-Faulkner, A. *et al.* Requirement of NOX2 and reactive oxygen species for efficient RIG-I-mediated antiviral response through regulation of MAVS expression. *PLoS pathogens* **6,** e1000930 (2010).

14. Kong, X., Thimmulappa, R., Kombairaju, P. & Biswal, S. NADPH oxidase-dependent reactive oxygen species mediate amplified TLR4 signaling and sepsis-induced mortality in Nrf2-deficient mice. *Journal of immunology (Baltimore, Md. : 1950)* **185,** 569–77 (2010).

15. Kobayashi, E. H. *et al.* Nrf2 suppresses macrophage inflammatory response by blocking proinflammatory cytokine transcription. *Nature communications* **7,** 11624 (2016).

16. Agod, Z. *et al.* Regulation of type I interferon responses by mitochondria-derived reactive oxygen species in plasmacytoid dendritic cells. *Redox biology* **13,** 633–645 (2017).

17. Yu, Y., Clippinger, A. J. & Alwine, J. C. Viral effects on metabolism: changes in glucose and glutamine utilization during human cytomegalovirus infection. *Trends in microbiology* **19,** 360–367 (2011).

18. Vastag, L., Koyuncu, E., Grady, S. L., Shenk, T. E. & Rabinowitz, J. D. Divergent effects of human cytomegalovirus and herpes simplex virus-1 on cellular metabolism. *PLoS pathogens* **7,** e1002124 (2011).

19. Sychev, Z. E. *et al.* Integrated systems biology analysis of KSHV latent infection reveals viral induction and reliance on peroxisome mediated lipid metabolism. *PLoS pathogens* **13,** e1006256 (2017).

20. Beltran, P. M. *et al.* Infection-Induced Peroxisome Biogenesis Is a Metabolic Strategy for Herpesvirus Replication. *Cell host & microbe* **24,** 526-541.e7 (2018).

21. Choi, Y. B., Choi, Y. & Harhaj, E. W. Peroxisomes support human herpesvirus 8 latency by stabilizing the viral oncogenic protein vFLIP via the MAVS-TRAF complex. *PLoS pathogens* **14,** e1007058 (2018).

22. Magalhães, A. C. *et al.* Peroxisomes are platforms for cytomegalovirus' evasion from the cellular immune response. *Scientific reports* **6,** 26028 (2016).

23. Zheng, C. & Su, C. Herpes simplex virus 1 infection dampens the immediate early antiviral innate immunity signaling from peroxisomes by tegument protein VP16. *Virology journal* **14,** 35 (2017).

24. Barton, E., Mandal, P. & Speck, S. H. Pathogenesis and host control of gammaherpesviruses: lessons from the mouse. *Annual review of immunology* **29,** 351–397 (2011).

25. Reese, T. *et al.* Helminth infection reactivates latent γ-herpesvirus via cytokine competition at a viral promoter. *Science* **345,** 573–577 (2014).

26. Reese, T. A. Co-infections: Another Variable in the Herpesvirus Latency-Reactivation Dynamic. *Journal of virology* **90,** JVI.01865-15-5537 (2016).

27. Reddy, J. & Hashimoto, T. Peroxisomal beta-oxidation and peroxisome proliferator-activated receptor alpha: an adaptive metabolic system. *Annual review of nutrition* **21,** 193–230 (2001).

28. Teissier, E. *et al.* Peroxisome proliferator-activated receptor alpha induces NADPH oxidase activity in macrophages, leading to the generation of LDL with PPAR-alpha activation properties. *Circulation research* **95,** 1174–82 (2004).

29. Nguyen, T., Nioi, P. & Pickett, C. B. The Nrf2-antioxidant response element signaling pathway and its activation by oxidative stress. *The Journal of biological chemistry* **284,** 13291–5 (2009).

30. Chan, K., Lu, R., Chang, J. & Kan, Y. NRF2, a member of the NFE2 family of transcription factors, is not essential for murine erythropoiesis, growth, and development. *Proceedings of the National Academy of Sciences of the United States of America* **93,** 13943–8 (1996).

31. Itoh, K. *et al.* An Nrf2/small Maf heterodimer mediates the induction of phase II detoxifying enzyme genes through antioxidant response elements. *Biochemical and biophysical research communications* **236,** 313–22 (1997).

32. McMahon, M. *et al.* The Cap'n'Collar basic leucine zipper transcription factor Nrf2 (NF-E2 p45-related factor 2) controls both constitutive and inducible expression of intestinal detoxification and glutathione biosynthetic enzymes. *Cancer research* **61,** 3299–307 (2001).

33. Dutia, B., Allen, D., Dyson, H. & Nash, A. Type I interferons and IRF-1 play a critical role in the control of a gammaherpesvirus infection. *Virology* **261,** 173–179

34. Hwang, S. *et al.* Persistent gammaherpesvirus replication and dynamic interaction with the host in vivo. *Journal of virology* **82,** 12498–12509 (2008).

35. den Bossche, J., O'Neill, L. A. & Menon, D. Macrophage Immunometabolism: Where Are We (Going)? *Trends in immunology* **38,** 395–406 (2017).

36. Hall, C. J. *et al.* Immunoresponsive gene 1 augments bactericidal activity of macrophage-lineage cells by regulating β-oxidation-dependent mitochondrial ROS production. *Cell metabolism* **18,** 265–78 (2013).

37. Moon, J.-S. S. *et al.* NOX4-dependent fatty acid oxidation promotes NLRP3 inflammasome activation in macrophages. *Nature medicine* **22,** 1002–12 (2016).

38. Bulua, A. C. *et al.* Mitochondrial reactive oxygen species promote production of proinflammatory cytokines and are elevated in TNFR1-associated periodic syndrome (TRAPS). *The Journal of experimental medicine* **208,** 519–33 (2011).

39. Dixit, E. *et al.* Peroxisomes are signaling platforms for antiviral innate immunity. *Cell* **141,** 668–81 (2010).

40. Odendall, C. *et al.* Diverse intracellular pathogens activate type III interferon expression from peroxisomes. *Nature immunology* **15,** 717–26 (2014).

41. Shang, G., Zhang, C., Chen, Z. J., Bai, X.-C. C. & Zhang, X. Cryo-EM structures of STING reveal its mechanism of activation by cyclic GMP-AMP. *Nature* **567,** 389–393 (2019).

42. Ergun, S. L., Fernandez, D., Weiss, T. M. & Li, L. STING Polymer Structure Reveals Mechanisms for Activation, Hyperactivation, and Inhibition. *Cell* **178,** 290-301.e10 (2019).

43. Jin, L., Lenz, L. L. & Cambier, J. C. Cellular reactive oxygen species inhibit MPYS induction of IFNβ. *PloS one* **5,** e15142 (2010).

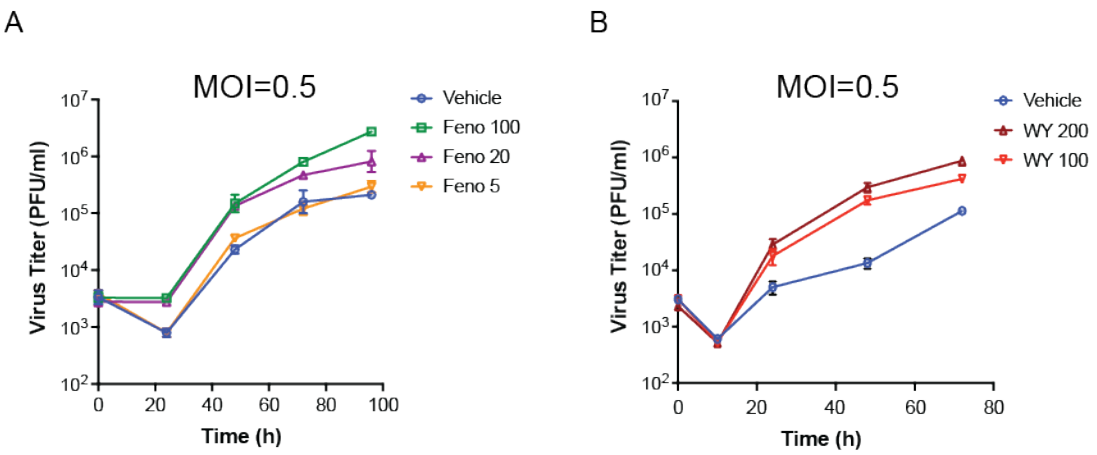

Supplemental Figure 1. Viral replication with different doses of fenofibrate and WY14643.

(A) Macrophages from C57BL6/J mice were treated with vehicle or increasing doses of fenofibrate (5, 20, or 100 μM) for 16 hours. Cells were infected with MHV68 at MOI=0.5 and viral growth was quantitated by plaque assay on 3T12 cells.

(B) Macrophages from C57BL6/J mice were treated with vehicle or increasing doses of WY14643 (100 or 200 μM) for 16 hours. Cells were infected with MHV68 at MOI=0.5 and viral growth was quantitated by plaque assay on 3T12 cells.

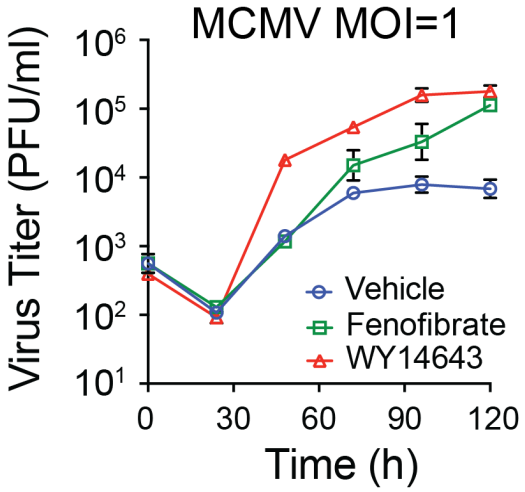

Supplemental Figure 2. PPAR-α stimulation increases virus replication of MCMV.

Growth curve of MCMV in macrophages isolated from C57BL/6J mice after pretreatment with vehicle, WY14643 or fenofibrate. Cells were infected with MCMV at MOI=1. Data represents mean ± SD from 2 independent experiments.

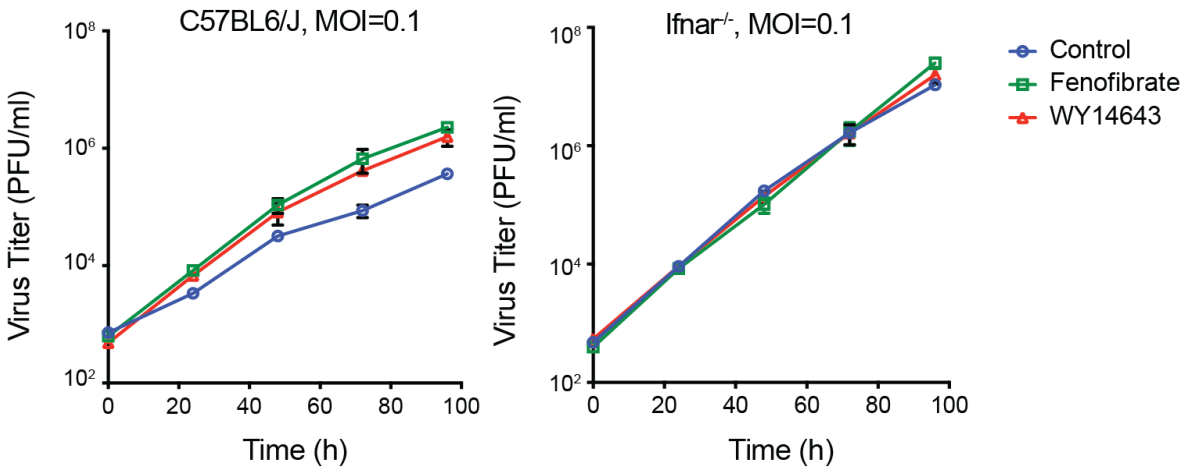

Supplemental Figure 3. Effects of PPAR-α stimulation are IFNAR-dependent.

Macrophages from C57BL6/J mice or *Ifnar*$^{-/-}$ mice were treated with vehicle, fenofibrate or WY14643 for 16 hours. Cells were infected with MHV68 at MOI=0.1 and viral growth was quantitated by plaque assay on 3T12 cells.

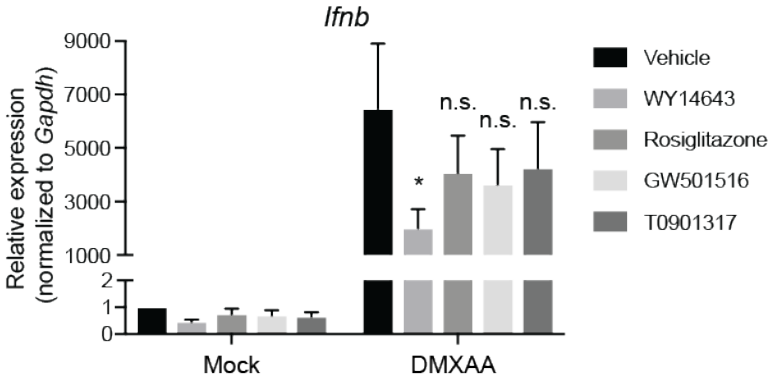

Supplemental Figure 4. *Ifnb* expression after treatment with PPAR-α, PPAR-γ, PPAR-δ, or LXR-α agonists. Macrophages from C57BL6/J mice were treated with vehicle, WY14643, rosiglitazone, GW501516, or T0901319 for 16 hours. Cells were then transfected with DMXAA and *Ifnb* expression was quantitated from lysates 2 hours after transfection. Expression was normalized to *Gapdh*. Data all shown as mean ± SD; $^{*}p<0.05$, n.s. (not significant), relative to DMXAA/vehicle treated. Statistical analysis was conducted using two-way ANOVA test.

Table 1. Differential expression of genes involved in innate inflammatory response

Gene	Mock			WY14643			MHV68			MHV68+WY14643			cGAS	PRR	NF-κB Signaling	IL-6 Signaling	Interferon Signaling	Acute Phase Response Signaling
	1	2	3	1	2	3	1	2	3	1	2	3						
IL18	214	181	177	166	184	187	2342	2438	1992	1720	1678	1694		√	√	√		√
TNF	1498	1498	2067	906	880	922	7828	7552	9224	2083	2178	2160		√	√	√		√
NFKBIE	1115	1114	1425	710	718	658	4615	4386	4872	1432	1454	1466		√	√	√		√
IL1RN	1340	1545	1464	547	527	514	5950	5147	5320	1755	1690	1957		√	√	√		√
IL1A	2	5	4	2	1	4	11	12	7	7	5	6		√	√	√		√
NFKBIB	1048	993	1001	701	639	693	2365	2360	2255	1204	1170	1239		√	√	√		√
NFKBID	467	454	580	579	581	587	1015	987	1250	638	761	644		√	√	√		√
TRAF2	645	642	665	534	543	561	1418	1407	1315	723	682	758		√	√	√		√
FGFR1	26	33	16	51	45	49	57	46	71	133	111	130		√	√	√		
PIK3R6	428	466	500	472	503	433	993	880	1068	690	669	631		√	√	√		
MYD88	2254	2195	2088	1965	2059	2004	9418	9895	9174	5842	5502	5838		√	√			√
TLR3	421	427	444	378	340	355	10029	8707	11218	5054	5306	5146		√	√			
EIF2AK2	1538	1482	1706	1108	1144	1171	12635	11494	14915	10992	10945	10909		√	√			
TLR2	10294	9509	11192	4098	4381	4192	32293	32202	32585	10216	9579	10529		√	√			
CASP8	2315	2384	2334	2862	2842	2834	6680	6252	6824	5428	5339	5493		√	√			
TNFSF13B	38	31	33	15	24	21	126	72	71	46	43	47		√	√			
TLR7	5389	5467	5714	3498	3413	3314	14199	12773	16330	9071	9016	9201		√	√			
TLR9	531	562	595	428	462	391	1478	962	1968	698	677	666		√	√			
TANK	1682	1676	1782	1158	1102	1181	4226	4062	4476	1977	1885	1965		√	√			
TLR8	3210	3237	3607	4598	4490	4216	7612	6779	9623	9866	9657	9574		√	√			
TLR6	469	466	455	461	421	416	974	867	987	703	601	687		√	√			
IL6	0	1	0	0	0	0	17	19	12	0	0	1		√		√		√
IKBKE	2727	2630	3106	2355	2312	2210	5996	5642	6981	3036	3082	3026		√		√		√
RASD2	6	6	5	6	4	3	10	10	16	6	6	10		√		√		√
IFNB1	1	1	0	0	0	0	44	34	35	1	0	5		√			√	
OAS3	1140	1141	1375	423	432	472	20896	17992	24239	17435	18349	17669		√			√	
OAS1G	189	233	200	82	89	104	3479	3341	3363	2206	2189	2223		√			√	
OAS1B	67	76	85	62	58	57	991	970	1181	640	774	728		√			√	
OAS1A	1021	1027	1007	453	448	473	11361	11963	10270	8194	7779	8206		√			√	

Gene	Mock			WY14643			MHV68			MHV68+WY14643			cGAS	PRR	NF-κB Signaling	IL-6 Signaling	Interferon Signaling	Acute Phase Response Signaling
	1	2	3	1	2	3	1	2	3	1	2	3						
OAS1C	117	111	92	86	77	74	798	912	774	578	581	601		√			√	
OAS2	756	766	1041	554	522	606	6160	4675	8929	5527	7345	5504		√			√	
C3	1174	1109	1159	479	499	448	13193	11612	15130	3365	3258	3503		√				√
TNFSF10	57	38	77	6	7	3	8736	8454	9395	3696	3442	3747		√				
CCL5	81	72	49	16	18	10	4182	4011	3520	437	368	437		√				
IRF7	772	815	783	150	173	159	41147	40260	40824	26639	26479	27343		√				
IFIH1	779	753	843	440	492	461	19733	19001	21380	11666	11350	11898		√				
TNFSF4	18	13	11	31	41	34	336	235	296	206	173	209		√				
DDX58	1163	1235	1444	624	600	595	22888	21147	26983	18054	18158	17569		√				
TNFSF15	11	14	7	3	3	4	181	180	208	39	38	37		√				
DHX58	914	946	913	474	423	431	14302	14384	14283	10439	10498	10630		√				
IL15	383	365	330	343	318	303	4611	5055	4337	2110	1883	2100		√				
TNFSF8	105	100	104	27	35	41	1236	1072	1240	442	470	499		√				
NOD1	270	264	288	308	303	294	2845	2959	3223	1535	1358	1616		√				
PRKCE	11	15	19	19	21	22	133	96	155	100	86	99		√				
TRAF1	150	168	186	71	73	77	1306	1071	1148	199	181	216		√				
NOD2	186	207	205	175	137	139	1270	1130	1498	584	502	521		√				
IL10	37	38	30	26	24	21	172	198	185	63	58	78		√				
CASP1	2087	2038	2095	1881	1871	1987	10078	10059	9223	6595	6505	6608		√				
RIPK2	488	508	503	397	450	428	1906	1971	2007	1025	868	990		√				
TRIM25	2609	2607	2681	3196	3243	3160	8390	7793	9505	7358	7478	7335		√				
IRAK2	1569	1516	1703	1172	1144	1118	4749	4796	4977	2506	2407	2619		√				
LTB	6	3	10	7	8	9	13	16	18	13	9	11		√				
UBC	1912	1952	2446	2259	2271	2144	5354	5568	4599	4788	4751	4965		√				
RELB	1280	1279	1423	643	676	648	2960	2877	3028	1235	1319	1394		√				
AKT3	1145	1188	1307	1350	1403	1392	4945	4111	5354	3544	3477	3528			√	√		√
TNFRSF1B	11046	10749	11198	11923	12072	11725	26748	24892	26938	21453	20583	22081			√	√		√
RAF1	2717	2725	2818	2829	2810	2989	5410	5632	5480	3984	3973	3967			√	√		√
IL1R2	16	20	17	6	8	11	46	64	48	48	24	44			√	√		
STAT3	2636	2581	2720	2997	3128	3133	6711	6102	7306	5448	5229	5591			√			√
FLT4	6	6	5	7	5	5	298	219	257	141	155	168			√			

Gene	Mock			WY14643			MHV68			MHV68+WY14643			cGAS	PRR	NF-κB Signaling	IL-6 Signaling	Interferon Signaling	Acute Phase Response Signaling
	1	2	3	1	2	3	1	2	3	1	2	3						
CD40	241	224	225	52	66	58	8145	8503	7354	2111	2001	2282			√			
KDR	459	502	491	158	190	167	6428	5838	7733	2610	2305	2611			√			
LCK	3	8	8	7	5	10	71	69	63	50	34	41			√			
FLT1	180	190	199	146	128	136	1388	1091	1428	737	675	603			√			
AZI2	1206	1171	1153	1122	1104	1165	5505	5316	5657	4208	4033	4081			√			
PELI1	1274	1231	1252	1057	1012	1060	5312	5420	5837	2669	2403	2658			√			
BMP2	24	23	21	5	5	7	70	76	109	22	8	16			√			
TNFAIP3	1394	1344	1533	743	713	674	4082	3777	4771	1402	1368	1419			√			
MAP3K8	248	238	255	321	312	290	615	625	660	430	407	464			√			
HDAC1	1141	1145	1196	1066	1040	1061	2699	2781	2588	1917	1923	1980			√			
SOCS1	28	33	30	23	20	14	953	1044	901	287	235	264				√	√	√
JAK2	919	925	1001	904	962	953	7304	6852	7891	4262	4168	4193				√	√	√
SOCS3	161	147	181	75	87	72	768	793	919	165	180	159				√	√	
CEBPB	1690	1677	1865	1568	1350	1260	5033	5023	5532	3049	3278	3081				√		√
IL1RAP	243	249	254	275	260	287	762	704	721	708	756	757				√		√
MAP2K1	4735	4703	4591	4638	4544	4542	11578	11466	11049	10140	9435	9856				√		√
TNFAIP6	0	1	0	1	1	1	20	18	5	6	2	8				√		
MCL1	13370	13145	14265	10744	10256	10032	36309	36405	37898	21989	22645	22945				√		
MAPKAPK2	7602	7229	7788	5230	5062	5124	19231	19768	19006	9309	9084	9768				√		
IL18RAP	93	98	81	127	129	132	183	173	200	114	92	111				√		
IFIT3	699	752	718	68	83	84	71547	76452	75258	52105	48862	51428					√	
ISG15	467	442	412	69	63	68	32503	34593	29861	18088	17179	18568					√	
STAT1	4405	4219	4528	2076	2201	2115	58462	59483	63427	49801	48886	49545					√	
TAP1	1796	1669	1594	1130	1211	1121	19657	20391	19816	13324	12700	13429					√	
IFI35	864	872	808	516	589	578	9556	10614	8826	6491	6282	6391					√	
STAT2	2294	2150	2473	2140	2086	2029	23292	21943	27767	21528	22535	21756					√	
IRF1	1456	1280	1410	877	902	870	9931	10321	11085	3871	3612	4169					√	
PSMB8	2270	2208	2023	1597	1730	1617	12367	13142	11161	8068	7882	8075					√	
IFITM3	6415	6793	6129	2309	2653	2393	28056	28253	24744	17039	16637	17767					√	
SOCS7	549	559	534	639	607	542	1951	1755	2336	998	969	1025					√	

Gene	Mock			WY14643			MHV68			MHV68+WY14643			cGAS	PRR	NF-κB Signaling	IL-6 Signaling	Interferon Signaling	Acute Phase Response Signaling
	1	2	3	1	2	3	1	2	3	1	2	3						
IRF9	1419	1387	1584	1027	977	1001	3698	3583	3662	3237	3324	3305					√	
TYK2	2458	2323	2598	2846	2750	2779	5953	4969	6582	4094	4265	4089					√	
CFB	49	57	51	30	35	43	1543	1481	1338	365	396	389						√
SOCS2	6	7	19	9	9	9	128	121	127	35	27	45						√
CP	68	62	72	30	30	20	458	372	441	70	82	70						√
C2	6	7	5	3	9	7	40	31	33	18	34	23						√
C1RA	59	64	44	32	32	26	232	191	202	87	98	108						√
HP	6	9	9	3	0	2	30	31	22	7	7	3						√
F8	10	10	9	9	4	3	28	38	32	15	15	8						√
TCF4	2157	2046	2139	2014	1969	1919	5627	5273	6623	3476	3550	3464						√
HMOX2	2103	2139	2025	1688	1745	1845	5653	5928	5272	4839	4635	4826						√
APOA2	4	7	3	5	4	1	11	11	8	7	4	5						√
NFKBIA	3201	3134	3526	2777	2672	2730	9695	10176	10278	4679	4668	4725	√	√	√	√		√
CASP12	3	2	1	0	1	0	41	41	44	16	16	13	√					
CASP4	403	346	464	201	202	221	4588	4483	4288	1987	1950	2141	√					
TREX1	1147	1150	1174	674	642	620	11338	12083	10822	6742	6376	7018	√					
SQSTM1	17196	16704	18097	24329	24385	23906	33074	33293	32163	36959	35126	37671	√					
TBK1	2377	2384	2397	2445	2400	2397	4357	4293	4487	3062	3230	3201	√					
CHUK	1441	1529	1573	1640	1608	1568	2029	1945	2083	1871	1823	1826	√					
MAP1LC3A	429	391	455	525	461	523	579	585	491	515	521	499	√					
BAX	3470	3327	3128	3226	3204	3212	4116	4459	3952	3809	3902	3871	√					
RPS6KB1	787	790	857	979	1006	968	779	752	875	834	863	832	√					
IRF3	1127	1158	1171	1314	1318	1297	1056	1150	1135	1128	1193	1141	√					
ULK1	976	933	1021	1419	1423	1376	550	451	674	913	881	831	√					

List of genes and their expression values across three biological replicates for each of the four groups (Vehicle-treated, WY14643-treated, MHV68-infected, and MHV68-infected/WY14643-treated). Membership of genes in various inflammatory pathways as defined by Ingenuity are listed.

Table 2. Differential expression of genes involved in cellular oxidative stress with WY14643 treatment

Gene	Mock			WY14643			Redox Metabolism	Iron Metabolism	Nrf2-Mediated Oxidative Stress	Antioxidant action of vitamin C
	1	2	3	4	5	6				
Txnrd1	4828	5101	4918	14630	14375	15191	√		√	
Cat	769	791	692	1777	1761	1810	√		√	
Gsr	9	16	11	92	97	96	√		√	
Gsta3	2029	2066	2272	4601	4581	4414	√		√	
Gstm1	26	27	13	35	46	46	√		√	
Gstp1	52	61	63	102	115	94	√		√	
Gstt2	1153	1030	1088	2740	2838	2751	√		√	
Mgst1	46	61	57	149	173	146	√		√	
Nqo1	25451	25969	25176	41463	42096	44113	√		√	
Prdx1	2764	2846	2704	4726	4787	4796	√		√	
Sod1	1529	1507	1545	2365	2413	2522	√		√	
Prdx6	171182	175383	170069	318219	297781	303528	√			
Ftl1	395	374	413	845	866	738		√	√	
Gdf15	3463	3641	3357	8580	8300	8575		√		
Slc11a1	1521	1513	1711	2765	2739	2793		√		
Slc25a37	3312	3349	2766	10243	10169	9856		√		
Slc40a1	7171	7229	7051	11446	11255	11091		√		
Slc48a1	23341	23271	21494	55598	51879	54662		√		
Hmox1	1514	1553	1775	3111	2875	2869			√	√
Fos	6	11	18	22	20	23			√	
Prkcg	4600	4834	4718	7321	7279	7459			√	
Abcc1	4	4	5	20	21	20			√	
Aox1	27	33	27	113	101	113			√	
Dnajb13	1735	1782	1732	3403	3358	3463			√	
Gclc	2141	2187	2058	7881	7657	8343			√	
Gclm	1757	1677	1801	2744	2639	2745			√	
Ikbkg	26	25	28	43	46	57				√
Abhd3	2762	2689	2970	5391	5051	5302				√

Gene	Mock			WY14643			Redox Metabolism	Iron Metabolism	Nrf2-Mediated Oxidative Stress	Antioxidant action of vitamin C
	1	2	3	4	5	6				
Csf2ra	807	791	741	1746	1631	1595				√
Pla2g7	7	6	7	2	3	0				√
Plb1	37	33	44	21	26	21				√
Pla2g2e	1498	1498	2067	906	880	922				√
Tnf	270	254	299	185	169	194				√
Plcb4	1115	1114	1425	710	718	658				√
Nfkbie	2674	2553	3021	1835	1808	1725				√
Nfkb2	839	915	987	106	128	149				√
Rsad2	248	241	250	141	128	122			√	
Maff	2481	2269	2687	1394	1483	1347			√	
Herpud1	126	152	112	85	64	69			√	
Acta2	6	9	9	3	0	2		√	√	
Hp	68	62	72	30	30	20		√		
Cp	7	9	8	3	4	1				
Sod3	4828	5101	4918	14630	14375	15191	√		√	

List of genes and their expression values across three biological replicates for vehicle-treated and WY14643-treated groups. Membership of genes in various oxidative stress pathways as defined by Ingenuity are listed.

Material and Methods

Animals

C57BL/6J, B6;129S4-*Ppar*$\alpha^{tm1Gonz}$/J, C57BL/6J-*Tmem173*^{gt}/J, B6(Cg)-*Tmem173*$^{tm1.2Camb}$/J, B6.129S2-*Ifnar1*^{tm1Agt}/Mmjax, and B6.129X1-*Nfe2l2*^{tm1Ywk}/J were purchased from The Jackson Laboratory. All mice were housed under specific pathogen-free, double-barrier facility at the University of Texas Southwestern Medical Center. Mice were fed autoclaved rodent feed and water. Mice were maintained and used under a protocol approved by UT Southwestern Medical Center Institutional Animal Care and Use Committee (IACUC).

Chemicals

For *in vitro* experiments, PPARα agonists, Fenofibrate and WY14643; PPARβ agonist, GW501516; PPARγ agonist, Rosiglitazone were purchased from Sigma. For *in vivo* experiments, WY14643 was purchased from Cayman. Hydrogen peroxide solution and N-Acetyl-L-Cysteine was purchased from Sigma.

Cell culture

Bone marrow derived macrophages were differentiated in DMEM (Corning) with 10% FBS supplemented with 1% glutamine (Corning), 1% HEPES (Corning) and 10% CMG14 supernatant for 7 days [1]. 3T12 cells were maintained in DMEM with 5% FBS supplemented with 1% glutamine and 1% HEPES.

Generation of virus stocks

Murine γ-herpesvirus 68 (WUSM stain) was purchased from ATCC. Murine γ-herpesvirus 68-M3FL was generated as previously reported [2].

Virus infection

Fully differentiated BMDMs were seeded on 24 well plates (1.5×10^5 cells per well) or 6 well plate (10^6 cells per well). Cells were pretreated with either vehicle control (0.1% DMSO) or agonists (Fenofibrate 50 μM, WY14643 200 μM, Rosiglitazone 1 μM, GW501516 100 nM) for 16 hours. The next days, macrophages were infected with MHV68 at multiplicity of infection (MOI)=5 or 0.1. For MCMV experiments, cells were infected at MOI=1. After an hour, cells were washed with PBS twice to remove unabsorbed viruses and resuspended in medium containing

treatments. For growth curve, samples were collected at 0 hour, 24 hours, 48 hours, 72 hours and 96 hours after infection and were frozen at -80 °C. The titer of virus was determined by plaque assay in 3T12 cells. For flow cytometric analysis, cells were collected 24 hours after infection.

Flow cytometry for MHV68 lytic proteins positive cells

To determine the percentage of cells that expressing lytic proteins of MHV68 infection, cells were harvested 24 hours after infection, and fixed with 2% formaldehyde, blocked with 10% mouse serum and 1% Fc block (CD16/32, BioLegend), then stained with polyclonal rabbit antibody to MHV68 (1:1000) [3,4], followed by secondary goat anti-rabbit Alexa Fluor-647 (Invitrogen).

Transfection

Cells were seeded on 6 well plates and treated as needed. Cells were transfected with STING ligand (DMXAA, 10 μg/ml, InvivoGen) using Lipofectamine 3000 (Thermo Fisher Scientific) according to the manufacturer's protocol.

Plaque assay

The concentration of virus was titered in 3T12 cells. The frozen samples containing viruses were thawed in incubator. The samples were serial diluted, then added to a monolayer of 3T12 cells. After an hour of absorption, the cells were then covered with 1% methylcellulose. Plates were incubated at 37 °C for 7 days, and the plaques were stained with 0.1% crystal violet.

Western blot

Cells were lysed with RIPA buffer (150 mM NaCl, 1% NP-40, 0.5% sodium deoxycholate, 0.1% SDS, 25 mM Tris with protease inhibitor cocktail). Protein concentration were determined using Bradford assay (Bio-Rad). Equal amounts of protein were mixed with 5×loading sample buffer, resolved by 4-12% Bis-Tris plus gels (Thermo Fisher Scientific), and transferred to nitrocellulose membrane. Proteins were labeled with primary antibodies against STING (1:1000, Catalogue no.13647S, Cell Signaling), TBK1 (1:1000, Catalogue no. 3504S, Cell Signaling), IRF3 (1:1000, Catalogue no. 4302S, Cell Signaling), pTBK1 (1:1000, Catalogue no. 5483S, Cell Signaling), pIRF3 (1:1000, Catalogue no. 4947S, Cell Signaling), PPARα (1:1000, Catalogue no. Sc-398394, Santa Cruz), SDHA (1:5000, Catalogue no. ab14715, Abcam), β-actin (1:5000, Catalogue no. A2228, Sigma). Secondary antibodies used are donkey-anti-rabbit (1:5000,

Catalogue no.711-035-152, Jackson ImmunoResearch Laboratory) and goat-anti-mouse peroxidase (1:5000, Catalogue no.115-035-174 Jackson ImmunoResearch Laboratory). Membranes were developed using Luminata Forte Western HRP substrate (Millipore).

RT-qPCR

BMDMs in 6 well plates were either infected with MHV68 at MOI=5 for 6 hours or transfected with STING ligand DMXAA at 10 μg/ml for 2 hours. RNA was extracted using Qiagen RNeasy Mini Kit (Qiagen) and reverse transcribed into cDNA using SuperScript VILO cDNA Synthesis Kit (Thermo Fisher Scientific). Relative quantification of target genes was determined using PowerUp SYBR Green Master Mix (Thermo Fisher Scientific) in a QuantStudio 7 Flex real time PCR system. Primers used for amplifying target genes are listed in Table 3.

IFNβ ELISA Assay

BMDMs were seeded in 24 well plates. The next day, cells were treated with either vehicle control or WY14643 for 16 hours. Cells were then transfected with 10 μg/ml DMXAA. Supernatant of cells were collected 24 hours after transfection and frozen at -80 °C. The concentration of IFNβ in the supernatant was determined with PBL IFN Beta ELISA Kit (PBL Assay Science).

Total ROS measurement

The total ROS production was determined using ROS-ID Total ROS detection kit (Enzo) according to the manufacture's protocol. Cells were seeded on 24 well plates, and treatment with indicated compounds or DMSO for 6 hours, followed by incubation with oxidative stress detection reagent for 30 mins at 37 °C. The fluorescence of the detection reagent upon oxidation was analyzed by flow cytometry using a FACSCalibur (BD Biosciences).

MHV68 acute replication in mouse

Experiments were carried out using 8-12 weeks old male mice under the protocol approved by IACUC. Mice were injected intraperitoneally with either vehicle control (15% HS15 in normal saline) or WY14643 (100 mg/kg) for 1 week starting from 3 days before virus infection. Mice were then infected with MHV68-M3FL at the dose of 10^6 PFU through intraperitoneal route [2,4]. To quantify virus-encoded luciferase expression, mice were weighed and injected with 150 mg/kg of D-Luciferin (GOLDBIO) prior to imaging using IVIS Lumina III In Vivo Imaging System

(PerkinElmer). Total flux (Photons/second) of the abdominal region was determined using Living Image software (PerkinElmer). Survival of the mice were recorded until 20 days after infection.

RNA seq and data analysis

RNA samples were extracted with RNeasy Mini Kit (Qiagen) and RNA library was prepared using TruSeq Stranded mRNA Sample Preparation Kit (Illumina). Samples were sequenced on NextSeq 500/500 sequencer (Illumina) with SE-85. RNA seq data is normalized and analyzed based on the use of "internal standards" [5] that characterize some aspects of the system's behavior, such as technical variability, as presented elsewhere [6,7]. The two-step normalization procedure and the Associative analysis functions are implemented in MATLAB (MathWorks, MA) and available from authors upon request. Functional analysis of identified genes was performed with Ingenuity Pathway Analysis (IPA; Ingenuity System). The sequencing data has been deposited in the European Nucleotide Archive under the accession number PRJEB33753.

QUANTIFICATION AND STATISTICAL ANALYSIS

All data are presented as mean ± SD. Statistical comparisons were performed using GraphPad Prism 7.0 software. Data were compared using unpaired two-tailed t test, one-way or two-way ANOVA. Statistical significance was set at $p < 0.05$. The numbers of independent replicates (n) are reported in the figure legends.

REFERENCES

1. Reese, T. *et al.* Helminth infection reactivates latent γ-herpesvirus via cytokine competition at a viral promoter. *Science* **345,** 573–577 (2014).

2. Weck, K. E. *et al.* Murine γ-herpesvirus 68 causes severe large-vessel arteritis in mice lacking interferon-γ responsiveness: A new model for virus-induced vascular disease. *Nature medicine* **3,** 1346–1353 (1997).

3. Hwang, S. *et al.* Persistent gammaherpesvirus replication and dynamic interaction with the host in vivo. *Journal of virology* **82,** 12498–12509 (2008).

4. Rocke, D. & Durbin, B. A model for measurement error for gene expression arrays. *Journal of*

computational biology : a journal of computational molecular cell biology **8,** 557–69 (2001).

5. Dozmorov, I. & Lefkovits, I. Internal standard-based analysis of microarray data. Part 1: analysis of differential gene expressions. *Nucleic acids research* **37,** 6323–39 (2009).

6. Dozmorov, I. & Centola, M. An associative analysis of gene expression array data. *Bioinformatics (Oxford, England)* **19,** 204–11 (2003).

Table 3. QPCR primers for target genes

Primers	Sequence
Ifnb forward	CAGCTCCAAGAAAGGACGAAC
Ifnb reverse	GGCAGTGTAACTCTTCTGCAT
Cxcl10 forward	TTAACGTCAGGCCAACAGAG
Cxcl10 reverse	GAGGGAAACCAGGAAAGATAGG
Isg15 forward	CAGGACGGTCTTACCCTTTCC
Isg15 reverse	AGGCTCGCTGCAGTTCTGTAC
Isg20 forward	CCATGGACTGTGAGATGGTG
Isg20 reverse	CTCGGGTCGGATGTACTTGT
Gapdh forward	GGGTGTGAACCACGAGAAATA
Gapdh reverse	GTCATGAGCCCTTCCACAAT
Mgst1 forward	CTGACGAGAAGGTGGAACG
Mgst1 reverse	AGATTCTGAAGTGCATGAGGG
Gsr forward	CACCGAGGAACTGGAGAATG
Gsr reverse	ATCTGGAATCATGGTCGTGG
Slc7a11 forward	TGGGCTACGTACTGACAAAC
Slc7a11 reverse	AAAGATCGGGACTGCTAATGAG
Gstm1 forward	CTATGATACTGGGATACTGGAACG
Gstm1 reverse	ACTTCTCATTCAGCCACTGG
Gclm forward	AATCAGCCCCGATTTAGTCAG
Gclm reverse	CGATCCTACAATGAACAGTTTTGC
Cd36 forward	GCGACATGATTAATGGCACAG
Cd36 reverse	GATCCGAACACAGCGTAGATAG